

SFGAN: Unsupervised Generative Adversarial Learning of 3D Scene Flow from the 3D Scene Self

Guangming Wang¹, Chaokang Jiang², Zehang Shen¹, Yanzi Miao², and Hesheng Wang³

¹Department of Automation, Shanghai Jiao Tong University

²Engineering Research Center of Intelligent Control for Underground Space, Ministry of Education, School of Information and Control Engineering, Advanced Robotics Research Center, China University of Mining and Technology

³Key Laboratory of System Control and Information Processing of Ministry of Education, Key Laboratory of Marine Intelligent Equipment and System of Ministry of Education, Shanghai Engineering Research Center of Intelligent Control and Management, Department of Automation, Shanghai Jiao Tong University

October 4, 2021

Abstract

3D scene flow presents the 3D motion of each point in the 3D space, which forms the fundamental 3D motion perception for autonomous driving and server robots. Although the RGBD camera or LiDAR capture discrete 3D points in space, the objects and motions usually are continuous in the macro world. That is, the objects keep themselves consistent as they flow from the current frame to the next frame. Based on this insight, the Generative Adversarial Networks (GAN) is utilized to self-learn 3D scene flow with no need for ground truth. The fake point cloud of the second frame is synthesized from the predicted scene flow and the point cloud of the first frame. The adversarial training of the generator and discriminator is realized through synthesizing indistinguishable fake point cloud and discriminating the real point cloud and the synthesized fake point cloud. The experiments on KITTI scene flow dataset show that our method realizes promising results without ground truth. Just like a human observing a real-world scene, the proposed approach is capable of determining the consistency of the scene at different moments in spite of the exact flow value of each point is unknown in advance.

Corresponding author(s) Email: wanghesheng@sjtu.edu.cn

ToC Figure

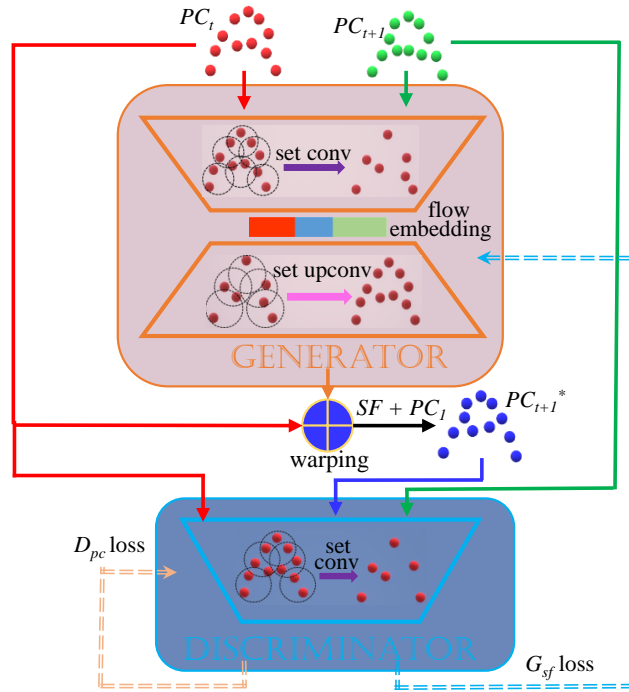


Figure 1: **ToC Figure.** Two point clouds PC_t and PC_{t+1} of consecutive frames are passed into the scene flow generator G_{sf} . G_{sf} consists of three parts: the learning of point cloud feature with the set conv layer, the learning of point relationship with the flow embedding layer, and the flow refinement with the set upconv layer. The point cloud PC_t at time t is warped to PC_{t+1}^* based on the predicted scene flow SF . PC_t , PC_{t+1} and PC_{t+1}^* are fed into our designed discriminator D_{pc} to predict the probability that the input point cloud is from the real point cloud. The G_{sf} loss and loss are designed to optimize G_{sf} and D_{pc} , respectively.

Introduction

Just like estimating 2D optical flow from a pair of images, estimating 3D scene flow from two frames of 3D point clouds is an fundamental task in computer vision and robot perception. 3D scene flow can be applied to object detection and tracking (Behl et al., 2017; Lenz et al., 2011; Zhai et al., 2020), LiDAR odometry (Wang et al., 2021e), action recognition (Wang et al., 2017), etc. Recently, some works (Liu et al., 2019a; Wang et al., 2021d; Puy et al., 2020; Li et al., 2021b,a; Wang et al., 2021a) have been done to realize supervised estimation of 3D scene flow from two consecutive frames of point clouds. However, just like it is difficult to obtain the ground truth of optical flow (Wang et al., 2021c, 2020b), the ground truth of 3D scene flow is also difficult to obtain. Therefore, it is essential to perform unsupervised learning of 3D scene flow.

Existing unsupervised learning methods for 3D scene flow always have some assumptions, which do not completely conform to the real situation. For example, the commonly used Chamfer loss (Wu et al., 2020; Kittenplon et al., 2021) for the unsupervised learning of scene flow aims to minimize the distance between the nearest points in both the predicted point cloud and the real point cloud, which assumes that the coordinates of the predicted point cloud of the second frame and the real point cloud of the second frame are exactly the same in geometric space. However, due to the discrete sampling of LiDAR, the points that characterize the same object do not correspond point by point. Chamfer loss violates the discreteness fact of the point clouds. The cycle consistency loss (Mittal et al., 2020) predicts the reverse flow in order to transform the predicted point cloud of the second frame into the position of the first frame, which minimizes the distance

between the nearest points in the predicted point cloud of the first frame and the real point cloud of the first frame. In order to make the estimated point cloud structure stable, (Mittal et al., 2020) modified the starting point of the reverse flow. This artificial manipulation for the raw data violates the real data distribution. The Laplacian regularization loss (Wu et al., 2020) uses nearest three points to interpolate the Laplacian coordinate vector of predicted point clouds from the real point clouds, which assumes the curvature of the local point cloud varies linearly. Unsupervised learning of 3D scene flow from raw data without assumptions is still a challenge.

In this paper, we use the scene flow estimation network as a generator and design a robust discriminator to discriminate the generated point clouds and the real point clouds. The ground truth is not utilized in the optimization of the scene flow generator. Just like human perception, the discriminator discriminates the consistency between the real 3D scene and the synthesized 3D scene to optimize the accuracy of the scene flow generator. Our main contributions in this work are shown as follows:

- A novel self-supervised learning framework for 3D scene flow is proposed, in which generative adversarial ideas are introduced to learn 3D scene flow. The adversarial learning between the scene flow generator and the point cloud discriminator makes the generated point clouds by the generator more and more like the real point clouds, thus making the scene flow estimation more and more accurate.
- Four different types of point cloud discriminators are designed, which can be used to discriminate whether the point clouds are from real data or generated data. The best discriminator structure is finally verified by ablation experiments.
- The experimental results in KITTI dataset (Geiger et al., 2012) demonstrate that the introduction of adversarial learning ideas in scene flow estimation is effective to improve the performance of scene flow estimation.

Our paper is divided into five sections in total. Section II shows the related work. Section III introduces our approach, describing the overall framework, the detailed structures of the scene flow generator and the point cloud discriminator, and their adversarial learning process, respectively. The experiments including training details, dataset description, evaluation metrics, result analysis, and ablation experiments are presented in Section IV. Section V shows the conclusion.

Related Work

3D scene flow is a 3D motion field formed by the movement of scenes in Euclidean space, which has an important role in the autonomous driving field (Menze and Geiger, 2015). Motion information is essential for the understanding of dynamic environments, but most sensors cannot directly collect motion information. Therefore, motion estimation from the perceived raw sensor data is an important issue in the research community.

Some previous works (Huguet and Devernay, 2007; Pons et al., 2007; Menze and Geiger, 2015; Cech et al., 2011) commonly use RGB data to estimate scene flow. Huguet et al. (Huguet and Devernay, 2007) predict scene flow through synthesizing optical flow between two adjacent frame and the estimated depth maps by dense stereo matching. Cech et al. (Cech et al., 2011) propose the simple seed growing algorithm, the basic principle of which is to find correspondences in small neighborhoods around the initial seed correspondence set. Based on this principle, the disparity of the stereo image and the optical flow between consecutive images are calculated. Many researchers have also worked on scene flow estimation tasks based on RGBD camera, which provide a depth channel for images. Some works (Herbst et al., 2013; Jaimez et al., 2015) extends the 2D approach to 3D to predict scene flow based on RGBD data. RGBD flow (Herbst et al., 2013) extends the two-frame variational 2D flow algorithm to 3D, and the predicted dense 3D flow is applied to rigid motion segmentation. RAFT-3D (Teed and Deng, 2021) estimates pixel-wise 3D motion on RGBD

data or stereo images. RAFT-3D (Teed and Deng, 2021) introduces rigid motion embeddings of pixel-wise SE3, which is based on the optical flow estimation framework, RAFT (Teed and Deng, 2020).

The introduction of PointNet (Qi et al., 2017a) has caused a wave of point cloud deep learning, which is the first deep model that processes raw 3D point clouds directly. PointNet (Qi et al., 2017a) learns the spatial encoding for each point of the input point clouds, then uses the features of all points to obtain a global point cloud feature, but lacks the extraction and processing of local features. The feature extraction layer of PointNet++ (Qi et al., 2017b) contains sampling layer, grouping layer, and pointnet layer, which provide the ability of local features extraction. Recently, some new feature learning methods (Thomas et al., 2019; Wang et al., 2020a) of point clouds are proposed, but they focus on the semantic segmentation task of a single frame. Recent learning based works (Liu et al., 2019a; Wu et al., 2020; Wang et al., 2021d) are devoted to recovering 3D scene flow directly from 3D point cloud data. FlowNet3D (Liu et al., 2019a) learns point cloud features based on PointNet++ (Qi et al., 2017b) and introduces a new flow embedding module to learn point motion. FlowNet3D (Liu et al., 2019a) is a classic supervised model that estimates 3D scene flow directly from raw point clouds. HPLFlowNet (Gu et al., 2019) uses bilateral convolutional layers as the base module and recovers the 3D scene flow using a similar structure to FlowNet3D. Inspired by the optical flow estimation framework, PWC-Net (Sun et al., 2018), PointPWC-Net (Wu et al., 2020) introduces a new cost volume layer based on PointConv (Wu et al., 2019) and estimates the 3D flow in a coarse-to-fine style. Wang et al. (Wang et al., 2021d) introduce a hierarchical attention network in the task of the scene flow estimation, and propose a new flow embedding with dual attention to learn 3D scene flow. In addition, MeteorNet (Liu et al., 2019b) and ASTA3DCNNs (Wang et al., 2021b) focus on the feature learning of multi-frame point clouds (more than three frames), while ours focuses on the motion relationship between two frames.

The ground truth of 3D scene flow in real world are difficult to obtain, which leads to the scarcity of labeled scene flow data. Therefore, self-supervised learning of scene flow has important research values for 3D scene perception. Some recent works (Wu et al., 2020; Mittal et al., 2020; Pontes et al., 2020; Tishchenko et al., 2020) have been done on unsupervised learning of scene flow. PointPWC-Net (Wu et al., 2020) introduces three self-supervised losses including Chamfer loss, smoothness constraint loss, and Laplacian regularization loss in their framework for scene flow learning. Mittal et al. (Mittal et al., 2020) propose nearest neighbor loss and cycle consistency loss for self-supervised learning of 3D scene flow, and achieve outstanding performance. Pontes et al. (Pontes et al., 2020) constrain non-rigid motion flow using graph Laplacian of raw point cloud, which embeds the topology of the point cloud to capture context information. Tishchenko et al. (Tishchenko et al., 2020) divide the self-supervised learning of scene flow into two steps: ego-motion flow is calculated based on the assumption that the LiDAR is moving and the scene is stationary, and then non-rigid flow is calculated based on the assumption that the LIDAR is stationary and the scene is moving.

Goodfellow et al. (Goodfellow et al., 2014) first propose GAN (Generative Adversarial Nets). GAN has powerful representation capabilities and is great at unsupervised learning and generating data. Many works migrate the training ideas of GAN to various research fields. GANVO (Almalioglu et al., 2019) introduces joint unsupervised learning of pose and depth maps based on GAN and proposes a novel adversarial technique to generate depth images without ground truth. PoseGAN (Liu et al., 2020) applies the idea of GAN to the camera localization framework. PoseGAN designs the image generator by pose-to-image based on a conditional discriminator to discriminate whether the image comes from generated or trained data. MFGAN (Jung et al., 2020) transfers beneficial features from bright scenes to poor lighting scenes based on GAN, and this style transfer approach improves performance in the visual odometry task.

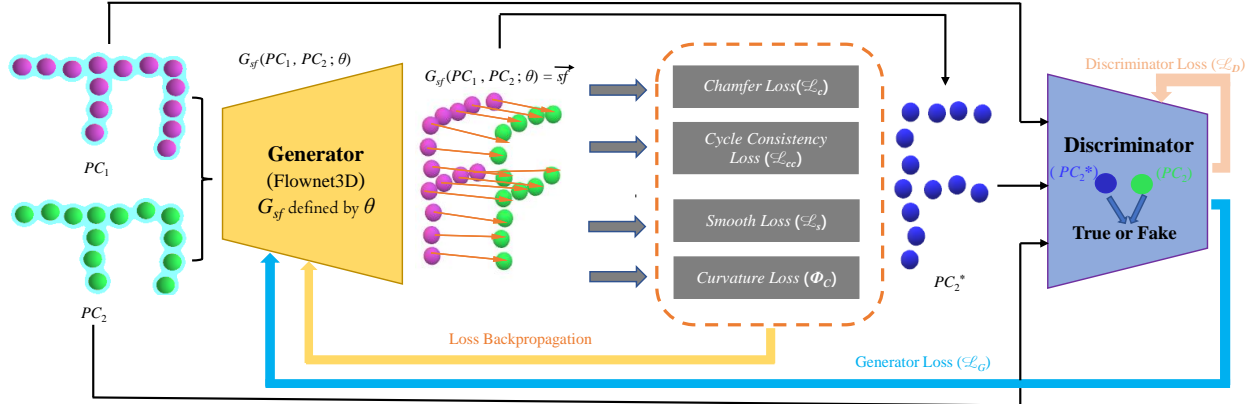


Figure 2: Overview of the proposed unsupervised adversarial learning framework of 3D Scene Flow. The point clouds of consecutive frames (purple point cloud PC_1 and green point cloud PC_2) are fed to the scene flow generator G_{sf} , and the output is the 3D scene flow SF for each point in point cloud PC_1 , with θ being the learnable parameter of G_{sf} . The predicted point cloud PC_2^* of the second frame is generated by scene flow warping ($PC_1 + SF$). Generator loss L_G and discriminator loss L_D are designed through the probabilities obtained from the point cloud discriminator, which are used to optimize the scene flow generator and point cloud discriminator, respectively.

SFGAN for Unsupervised Generative Adversarial Learning of 3D Scene Flow

In this section, a new unsupervised learning structure of 3D scene flow, SFGAN, is proposed. As shown in Figure 2, we introduce the game idea of GAN (Generative Adversarial Network) into unsupervised 3D scene flow learning. The new structure includes a scene flow generator G_{sf} and a point cloud discriminator D_{pc} . The generator G_{sf} learns the 3D scene flow SF from a pair of point clouds, the point cloud PC_1 of the first frame and the point cloud PC_2 of the second frame. The predicted point cloud PC_2^* of the second frame can be synthesized based on the learned scene flow SF and the point cloud PC_1 of the first frame. The designed discriminator can discriminate the probability of the point cloud being real data. The discriminator considers PC_2^* as a fake point cloud. The output probability value of the discriminator reflects the degree of truth of the input point cloud data. A higher probability value represents the greater possibility that the input point cloud is from real data. The range of the probability value is 0 to 1. The discriminator plays the adversarial role against the generator. The estimated accuracy of the 3D scene flow is continuously improved in the process of adversarial learning. Details of the model structure are presented in the following subsections.

Scene Flow Generator

The first part of the proposed model is to directly estimate the 3D scene flow from the raw point cloud pair by the scene flow generator G_{sf} , which is based on the FlowNet3D (Liu et al., 2019a). The detailed structure of the generator is shown in the upper part of Figure 3. The set conv layer processes a point cloud $PC = \{c_i, pf_i | i = 1, 2, \dots, n\}$ and returns a new point cloud $PC' = \{c'_j, pf'_j | j = 1, 2, \dots, m\}$. $c_i \in \mathbb{R}^3$ means the XYZ coordinate of a point. $pf_i \in \mathbb{R}^l$ represents the features of the point. l means the feature dimension of the point cloud. c'_j is the updated coordinate after the set conv layer. $pf'_j \in \mathbb{R}^{l'}$ is the updated point cloud feature, where l' is the updated feature dimension. The flow embedding layer learns a flow embedding d_k between PC_1 and PC_2 for each point in PC_1 . The output of the flow embedding layer is

represented as $\{c_k, d_k | k = 1, 2, \dots, n\}$, where $d_k \in \mathbb{R}^{l_1}$. l_1 means the dimension of flow embedding feature. Then, the flow embedding from the last step is up-sampled to the original point. This upsampling process is implemented through the learnable set upconv layer. The learnable upconv layer propagates flow embedding by aggregating features of neighboring points. The upconv layer learns how to weight the features of nearby points during network training. The scene flow $\vec{s}f$ of the raw point is predicted in the last layer, which is realized by the Full Connection (FC) layer.

Scene Flow Warping

As shown in Figure 2, we can generate the predicted point cloud PC_2^* of the second frame according to the predicted scene flow SF . The predicted scene flow from the generator G_{sf} is represented as $SF = \{\vec{s}f_i \in \mathbb{R}^3\}_{i=1}^{N_1}$. Predicted point cloud PC_2^* is synthesized from the point cloud $PC_1 = \{pc_{1,i} \in \mathbb{R}^3\}_{i=1}^{N_1}$ of the first frame and the predicted scene flow SF . The formula for the synthesis process is as follows:

$$PC_2^* = \{pc_{2,i}^* = pc_{1,i} + \vec{s}f_i | pc_{1,i} \in PC_1, \vec{s}f_i \in SF\}_{i=1}^{N_1}. \quad (1)$$

3D Structure Consistency

As shown in Figure 2, the scene flow generator G_{sf} is the main object of optimization in the whole network. A total of 5 loss functions are adopted to optimize the scene flow generator G_{sf} . They are Chamfer loss L_C , Laplacian regularization loss Φ_C , smooth loss L_S , cycle consistency loss L_{CC} , and GAN loss L_G . The first four loss functions are originated from existing unsupervised learning works (Wu et al., 2020; Mittal et al., 2020).

The estimated point cloud PC_2^* is synthesized by scene flow warping. The distance between PC_2 and PC_2^* is calculated by the sum of the distance from nearest point in PC_2^* to each point pc_2 of PC_2 and the distance from nearest point in PC_2 to each point pc_2^* of PC_2^* . The purpose of Chamfer loss is to minimize the distance between point cloud PC_2^* and point cloud PC_2 . The Chamfer loss L_C is defined as the following:

$$L_C(PC_2^*, PC_2) = \sum_{pc_2^* \in PC_2^*} \min_{pc_2 \in PC_2} \|pc_2^* - pc_2\|_2^2 + \sum_{pc_2 \in PC_2} \min_{pc_2^* \in PC_2^*} \|pc_2^* - pc_2\|_2^2. \quad (2)$$

To prevent large differences of the scene flow within a local space and to keep local smoothing, smooth loss function $L_S(D)$ assumes that the scene flow $SF(pc_i)$ at a point pc_i should be similar to the scene flow $SF(pc_j)$ at a point pc_j in the local space $N(pc_i)$ of pc_i . $N(pc_i)$ represents a local space around the point pc_i . $\|N(pc_i)\|$ represents the number of points in $N(pc_i)$. The detailed calculation process of L_S is as follows:

$$L_S(D) = \sum_{pc_i \in PC_1} \frac{1}{\|N(pc_i)\|} \sum_{pc_j \in N(pc_i)} \|SF(pc_j) - SF(pc_i)\|_2^2. \quad (3)$$

The points in the 3D point cloud exist only on the surface of the object due to the nature of LiDAR or RGB-D camera. The Laplacian regularization loss aims that the surface features of the predicted point cloud should be similar to that of the real point cloud. The difference degree of the surface feature is measured by comparing the Laplace coordinate vector of the predicted and real points. The Laplace coordinate vector is calculated as follows:

$$\delta(pc_i) = \frac{1}{\|N(pc_i)\|} \sum_{pc_j \in N(pc_i)} (pc_j - pc_i). \quad (4)$$

The Laplacian coordinate vector of the predicted point and the Laplacian coordinate vector of the real point should be the same. The interpolated Laplacian coordinate vector $\widehat{\delta}(pc_2^*)$ is obtained in order to directly compare the Laplacian coordinate vector of PC_2^* and PC_2 (Wu et al., 2020). The Laplacian regularization loss is defined as follows:

$$\Phi_C(\delta(pc_2^*), \widehat{\delta}(pc_2^*)) = \sum_{pc_2^* \in PC_2^*} \left\| \delta(pc_2^*) - \widehat{\delta}(pc_2^*) \right\|_2^2. \quad (5)$$

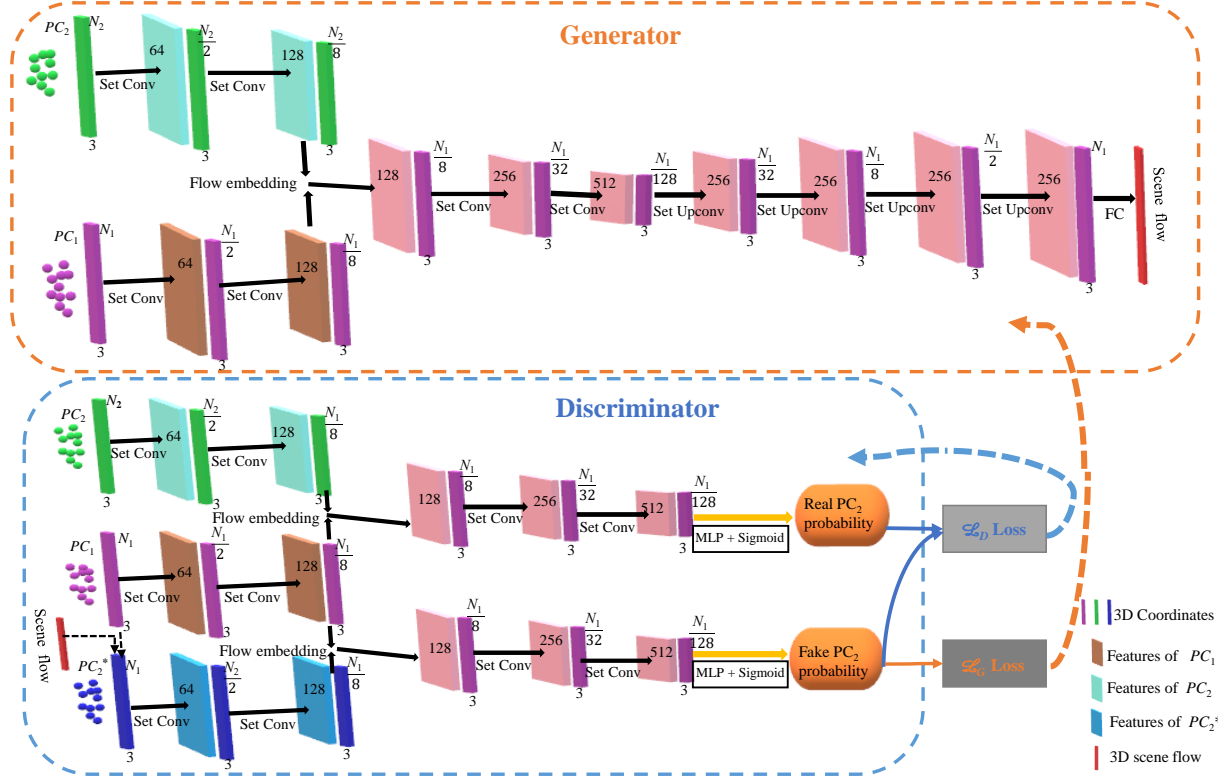


Figure 3: Adversarial learning network framework for 3D scene flow estimation. The FlowNet3D (Liu et al., 2019a) architecture is used as a generator to predict the scene flow at each point of PC_1 and to obtain PC_2^* . The discriminator generates the probability that PC_2 is true and the probability that PC_2^* is true, from which the loss functions are designed to train the generator and the discriminator respectively. FC represents fully connected layer.

According to the predicted scene flow $\vec{s}f$, the coordinates c_i of point $pc_{1,i}$ can be transformed to the coordinates c'_i of point $pc_{2,i}$. On the contrary, the reverse 3D scene flow sf'_i can be estimated based on PC_2^* and PC_1 . Based on PC_2^* and the reverse flow sf'_i , the predicted point cloud PC_1^* of the first frame can be synthesized. The aim of the cycle consistency loss L_{CC} is to minimize the distance between the predicted point cloud PC_1^* and the real point cloud PC_1 . In order to make the reverse 3D scene flow sf'_i estimation more stable and reliable, a new point cloud $\widehat{PC}_2 = \{\widehat{pc}_{2,i} \in \mathbb{R}^3\}_{i=1}^{N_1}$ of the second frame is created from PC_2 and PC_2^* , where $\widehat{pc}_{2,i}$ is computed through the convex combination (Mittal et al., 2020) of $pc_{2,i}$ and its nearest neighbor $pc_{2,j}$. Finally the coordinates c''_i of the predicted point cloud PC_1^* are obtained. The goal of the cycle consistency loss L_{CC} is to minimize the distance between coordinate c_i and coordinate c''_i , which is defined as follows:

$$L_{CC} = \sum_i^N \|c''_i - c_i\|^2. \quad (6)$$

As shown in the bottom half of Figure 3, the discriminator D_{pc} discriminates the predicted point cloud PC_2^* and the real point cloud PC_2 at the same time and outputs two probability values. More details of the discriminator will be described in the next subsection. The purpose of the scene flow generator G_{sf} is to produce a more accurate 3D scene flow that can fool the discriminator. In the training process of the network, error of data distribution is produced when the distribution P_g of the generated data is fitted to the distribution P of the real data. The loss function based on the distribution error is designed to optimize

G_{sf} by back propagation.

The original GAN randomly samples z from noise prior $Q_g(z)$ and the sampled samples are fed into the generator network G to generate new data $G(z)$. In our work, point clouds of consecutive frames are passed into the scene flow generator G_{sf} , and the predicted 3D scene flow SF is returned. The predicted PC_2^* is synthesized from the PC_1 and the prediction flow $\vec{s}f$. pc_2^* is the sample from the generated data distribution $P_g(pc_2^*)$. The discriminator D_{pc} discriminates the generated point cloud and generates a probability value of the point cloud coming from the real data, where the probability value reflects the difference between the generated data and the real data. The goal of G_{sf} is to minimize the difference, which means maximizing probability $D_{pc}(pc_2^*)$. the GAN loss function L_G is defined as follows:

$$L_G = \mathbb{E}_{pc_2^* \sim P_g(pc_2^*)} [\log(D_{pc}(pc_2^*))]. \quad (7)$$

Five loss functions work together to optimize the scene flow generator G_{sf} . Each loss function has its own weight factor. The total loss function of the generator G_{sf} is shown as follows:

$$L_{total} = \lambda_c L_C + \lambda_s L_S + \lambda_\Phi \Phi_C + \lambda_{cc} L_{CC} + \lambda_g L_G, \quad (8)$$

where λ_c , λ_s , λ_Φ , λ_{cc} , and λ_g represent the weight of each loss.

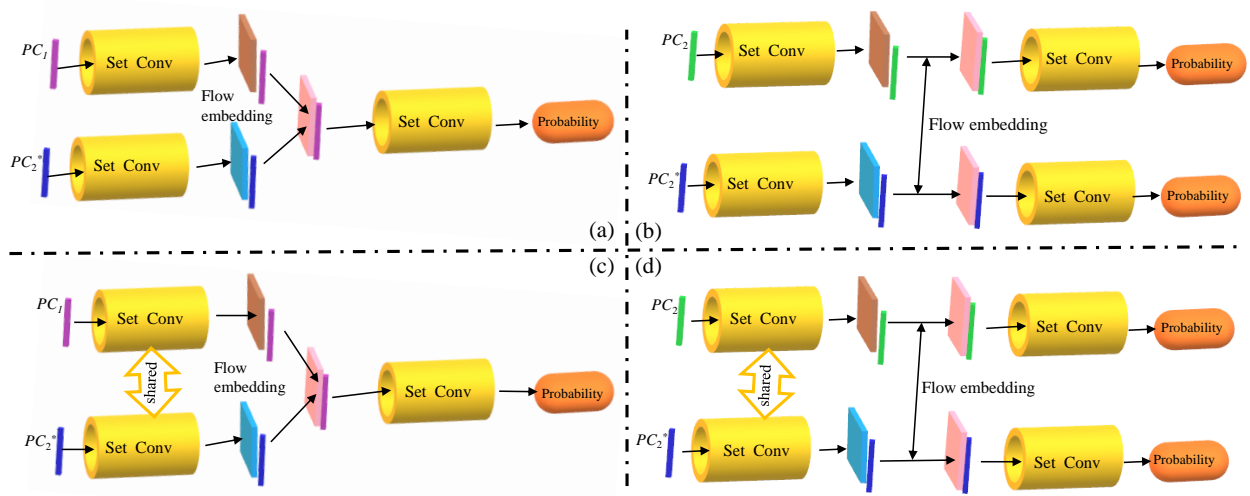


Figure 4: Different discriminator designs. Feature extraction layers of discriminator (a)(b) are set to not share weights, while discriminator (c)(d) share weights during feature extraction. Discriminator (a)(c) performs flow embedding with PC_1 and PC_2^* . Unlike discriminator (a)(c), discriminator (b)(d) perform feature embedding using PC_2 and PC_2^* .

Structural Similarity Discriminator

In pursuit of better discrimination, we design four different discriminator structures, which can be divided into (a)(b) and (c)(d) in Figure 4 according to whether the feature extraction layers of the point cloud share weights. According to the predicted point cloud PC_2^* with PC_1 or PC_2 for flow embedding, the four discriminators are classified into two kinds, (a)(c) and (b)(d). In the (a)(c) structure, PC_2^* performs flow embedding with PC_1 . In the (b)(d) structure, PC_2^* performs flow embedding with PC_2 . In experiment part, we will discuss the advantages and disadvantages of the four discriminators with the experiments. The best discriminator structure is determined by ablation experiments. As shown in the bottom half of Figure 3, PC_1 , PC_2 , and PC_2^* are fed into the discriminator. First, the input point cloud is downsampled, and

the soft correspondence of each point in PC_1 is found in PC_2 or PC_2^* by the flow embedding layer. After learning the flow embedding for each point in PC_1 , we continue to downsample using the set conv layer. Lastly, the probability of the point cloud is calculated directly by the Multi-Layer Perceptron (MLP) and the Sigmoid function. Due to the same internal structure as the former except for the input, the structure of PC_1 perform flow embedding with PC_2 is not shown in Figure 4.

Generator and discriminator are trained by optimizing the loss function. In fact, they separately have their own loss functions. The real data pc_2 and the generated data pc_2^* by G_{sf} are fed into the D_{pc} together for true-false discrimination. The aim of training the discriminator D_{pc} is to maximize the probability $\log(D_{pc}(PC_2))$ and maximize the difference $\log(1 - D_{pc}(PC_2^*))$ between the data distribution $P_g(pc_2^*)$ of PC_2^* and the data distribution $P(pc)$ of PC_2 . As the discriminative capability of D_{pc} becomes more and more powerful, an balance is eventually reached, which ensures that the point cloud data distribution generated by G_{sf} belongs to the same as the real data distribution of the point cloud. Therefore, better performance of the point cloud discriminator D_{pc} results in superior performance of the scene flow generator G_{sf} . The discriminator loss L_D is defined as follows:

$$L_D = \max\{\mathbb{E}_{pc_2^* \sim P_g(pc_2^*)}[\log(1 - D_{pc}(pc_2^*))] + \mathbb{E}_{pc \sim P(pc)}[\log(D_{pc}(pc))]\}. \quad (9)$$

The Adversarial Training

In the proposed unsupervised framework of scene flow estimation, the scene flow generator and the point cloud discriminator are trained alternately. In the adversarial learning process, the scene flow generator and the point cloud discriminator play a minimax game. Poor discriminator performance at the beginning of training can cause the generator to develop in a bad trend. Therefore, discriminator D_{pc} should learn earlier than generator G_{sf} . At the beginning of training, although the predicted point cloud data is in the same feature space as the real point cloud data, the differences of their distributions are obvious. Therefore, the discriminator can easily distinguish the two. In the training phase of the generator G_{sf} , the L_G based on the probability generated from the discriminator is used to optimize the generator, which makes the distribution of the predicted fake point cloud gradually coincide with the distribution of the real point cloud, and the degree of difference between both is represented by $V(G_{sf}, D_{pc})$. In adversarial learning process of the two models, the goal of D_{pc} is to make $V(G_{sf}, D_{pc})$ as large as possible and the goal of G_{sf} is to make $V(G_{sf}, D_{pc})$ as small as possible. The process of the game for G_{sf} and D_{pc} is as follows:

$$\min_{G_{sf}} \max_{D_{pc}} V(G_{sf}, D_{pc}) = \mathbb{E}_{pc \sim P(pc)}[\log(D_{pc}(pc))] + \mathbb{E}_{pc^* \sim P_g(pc^*)}[\log(1 - D_{pc}(pc^*))]. \quad (10)$$

Experiments

We implement experiments with different training methods and run self-supervised training on different datasets. The initial model is trained on a large synthetic dataset at first. Unsupervised fine-tuning and supervised fine-tuning are run on a real dataset. Next, we explore the influence of each loss function on the model by ablation experiments, and also discuss the influence of loss weights of GAN. We design four different discriminators of the point cloud. The effects of the different discriminators on the results are also compared in the ablation experiments.

Implementation Details

Our model is pre-trained on the FlyingThing3D (Mayer et al., 2016) by means of self-supervised learning. The network framework is mainly based on FlowNet3D (Liu et al., 2019a). The pre-trained model is fine-tuned in the KITTI dataset (Geiger et al., 2012). A pair of point clouds containing 2048 points for each frame are input to the scene flow generator and the point cloud discriminator. The input feature of the raw point cloud is given as 0. The generator and the discriminator are trained, separately. The alternate training

with one epoch interval between generator and discriminator is most beneficial for the learning of 3D scene flow.

The whole network framework in this paper is built based on the deep learning framework, TensorFlow. Our model is trained on an NVIDIA GeForce RTX 2080Ti GPU, with the Adam optimizer (Kingma and Ba, 2014) used to optimize the network weights. The settings for each parameter of the Adam optimizer are a learning rate of 0.01, $\beta_1 = 0.9$, $\beta_2 = 0.999$, and a batch size of 4. The generator and the discriminator have the same optimizer configuration.

Datasets and Data Preprocessing

FlyingThings3D

The dataset contains about 32000 stereo images, where each pair of stereo images has its corresponding ground-truth optical flow map and ground-truth disparity map. The images in FlyingThings3D (Mayer et al., 2016) are synthesized by randomly sampling multiple moving objects from ShapeNet (Chang et al., 2015). We randomly selected 20000 samples from FlyingThings3D (Mayer et al., 2016) as the train set for our model. Our model predicts the scene flow directly from the 3D point cloud instead of RGB images. We use the same data preprocessing approach as FlowNet3D (Liu et al., 2019a). 3D point cloud pairs and ground truth scene flow are generated from ground truth disparity maps and ground truth optical flow. The generated paired 3D point clouds are used for the self-supervised learning of scene flow.

KITTI Scene Flow 2015 dataset

In the KITTI scene flow 2015 (Geiger et al., 2012), the scene flow vector is stored by two frames of the disparity maps and an optical flow map. There are 150 ground truth of 3D scene flow. We select 100 scenes for training, and the remaining 50 scenes are used for the evaluation. The ground points for each scene are removed, like the data pre-processing as FlowNet3D (Liu et al., 2019a).

Results and Analysis

The estimation results of the 3D scene flow are evaluated by using the data with scene flow annotations on KITTI. We quantitatively evaluate the results of the predicted scene flow using four metrics. EPE3D represents the average error of the predicted scene flow in meters, which is expressed by the following equation:

$\frac{1}{N_1} \sum_{i=1}^{N_1} \left\| \widehat{sf}_i - sf_i \right\|$, where N_1 represents the total number of scene flow. Accuracy of scene flow estimation is measured with ACC3D and Outliers3D. ACC3D includes the absolute and relative errors of the scene flow, and two thresholds are set for the errors. ACC3D Strict specifically is expressed as: $\left\| \widehat{sf}_i - sf_i \right\| < 0.05$ or $\frac{\left\| \widehat{sf}_i - sf_i \right\|}{sf_i} < 5\%$; ACC3D Relax specifically is expressed as: $\left\| \widehat{sf}_i - sf_i \right\| < 0.1$ or $\frac{\left\| \widehat{sf}_i - sf_i \right\|}{sf_i} < 10\%$. Outliers3D represents the percentage of scene flow with large errors. Outliers3D specifically is expressed as: $\left\| \widehat{sf}_i - sf_i \right\| > 0.3$ or $\frac{\left\| \widehat{sf}_i - sf_i \right\|}{sf_i} > 10\%$.

As shown in Table 1, first SFGAN obtains a pretrained model on FlyingThings3D. The fine-tuned model supervised in the KITTI dataset achieves remarkable results. In no access to the ground truth of the scene flow on the KITTI dataset, the pre-trained model is fine-tuned using our method with a self-supervised manner. SFGAN has a significant improvement on the metric EPE3D, surpassing the existing self-supervised fine-tuning methods (Mittal et al., 2020; Wu et al., 2020). The metric EPE3D reflects the global mean error of the predicted scene flow. In fact, when compared with other methods of unsupervised learning of scene flow, SFGAN has its own special characteristic. Chamfer loss (Wu et al., 2020) and cycle consistency loss (Mittal et al., 2020) are designed to match predicted and real points based on point-by-point correspondence, which violates the discrete sampling nature of point clouds. This assumption makes the error always present

Table 1: **Table 1** Evaluation results of the scene flow estimation in the KITTI dataset. ‘ \uparrow ’ represents larger values as better and ‘ \downarrow ’ represents smaller values as better. W_{gan} represents the weight coefficient of the GAN loss function. ‘Full’ represents the model with supervised learning on the FlyingThings3D. ‘Self + Full ft’ represents the model with Self-supervised learning on the FlyingThings3D and then with supervised fine-tuning on the KITTI dataset. ‘Self + Self ft’ represents the model with self-supervised training on the FlyingThings3D and then with self-supervised fine-tuning on the KITTI dataset.

Method	Sup.	EPE3D \downarrow	Acc3D Strict \uparrow	Acc3D Relax \uparrow	Outliers \downarrow
FlowNet3D (Liu et al., 2019a)	Full	0.183	0.0980	0.3945	0.7993
Mittal et al. (Mittal et al., 2020)	Self + Full ft	0.100	0.3142	0.6612	-
Our	Self + Full ft	0.075	0.4980	0.8117	0.4530
PointPWC-Net (Wu et al., 2020)	Self + Self ft	0.163	0.2117	0.5409	0.6934
Mittal et al. (Mittal et al., 2020)	Self + Self ft	0.126	0.3200	0.7364	-
Our ($W_{gan}=2$)	Self + Self ft	0.098	0.3022	0.6823	0.5584
Our ($W_{gan}=3$)	Self + Self ft	0.102	0.3205	0.6854	0.5532

in the self-supervised learning. The loss function of SFGAN compares the overall data distribution of the predicted point cloud and the real point cloud without assumption. The experiments demonstrate that the combination of the our proposed losses and original losses achieves the best model performance. The metric EPE3D is less than $0.1m$ without accessing the ground truth of scene flow. In addition, SFGAN outperforms Mittal et al. (Mittal et al., 2020) on the metric ACC3D Strict.

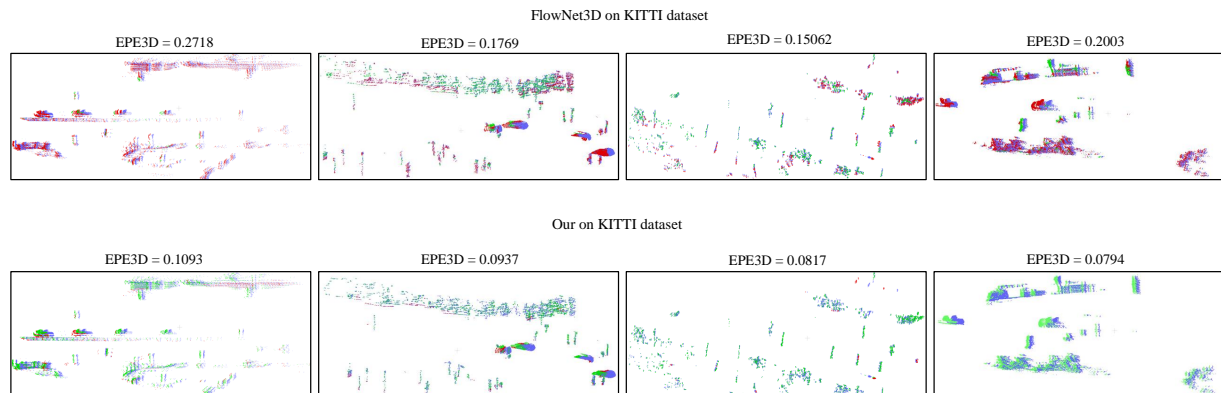


Figure 5: Visualization of the accuracy of 3D scene flow evaluation on the KITTI dataset. The top half shows the evaluation results of the predicted scene flow from FlowNet3D (Liu et al., 2019a), and the bottom half shows the evaluation results of the predicted scene flow from our model. PC_1 is represented by the blue points. the predicted point cloud PC_2^* synthesized from the predicted flow sf and PC_1 . We categorized the predicted points into incorrect points and correct points utilizing the Acc3D Relax metric. Correct points are shown in green and incorrect points are shown in red. We evaluated all points of the whole scene.

Figure 5 and Figure 6 show the visualization of the scene flow estimation for our method and FlowNet3D (Liu et al., 2019a). Our self-supervised method has better estimation results compared to FlowNet3D (Liu et al., 2019a). As shown in Figure 6, the point cloud (red) PC_2^* predicted by our method is highly similar in geometric shape to the real point cloud (green) PC_2 of the second frame.

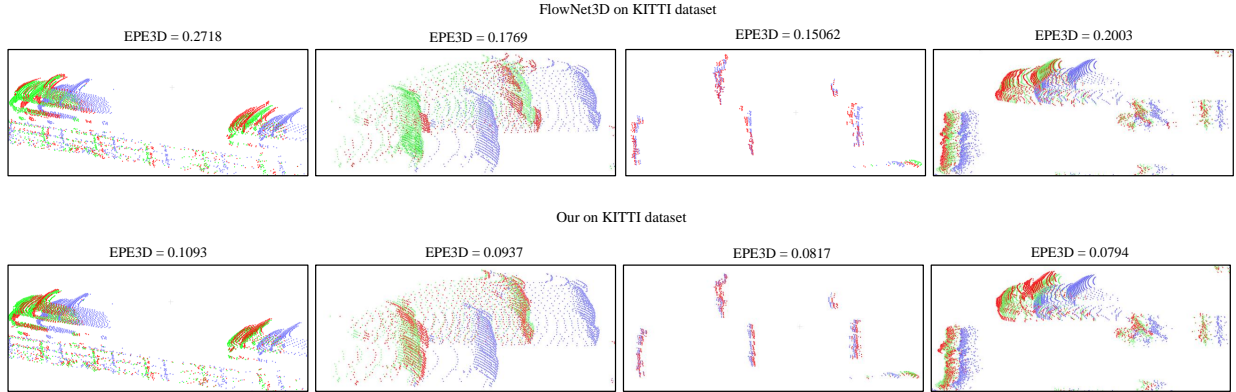


Figure 6: Detailed visualization of scene flow estimation on KITTI dataset. The top half shows the prediction results of the scene flow of FlowNet3D (Liu et al., 2019a). The bottom half shows the prediction results of scene flow of our method. PC_1 is blue points. The predicted point cloud PC_2^* and PC_2 are red points and green points, respectively.

Ablation Studies

The main focus of this section is to perform a series of ablation experiments on the loss function and point cloud discriminator of our network framework. Ablation studies include the contribution of each loss function, the effect of different weights of GAN loss functions, and the effect of four different discriminators, to the scene flow estimation.

Table 2: **Table 2** Ablation experiments on loss functions. Although these existing self-supervised loss functions have some drawbacks, their advantages can still improve the performance of scene flow estimation. Our method takes a different perspective and complements the other loss functions. The effect of different self-supervised losses on the evaluation results is studied.

L_C	L_{CC}	L_S	Φ_C	L_{GAN}	EPE3D↓	Acc3D Strict↑	Acc3D Relax↑	Outliers↓
-	✓	✓	✓	✓	0.4061	0.0072	0.0775	0.9979
✓	-	✓	✓	✓	0.4269	0.0029	0.0166	0.9839
✓	✓	-	✓	✓	0.1314	0.1576	0.5463	0.6805
✓	✓	✓	-	✓	0.1218	0.1822	0.5470	0.6929
✓	✓	✓	✓	-	0.1194	0.1851	0.5812	0.6571
✓	✓	✓	✓	✓	0.0987	0.3022	0.6823	0.5584

In this paper, five self-supervised losses including Chamfer Loss L_C , Laplacian regularization loss Φ_C , Smooth Loss L_S , Cycle Consistency Loss L_{CC} , and GAN Loss L_{GAN} are used to train the scene flow generator. As shown in Table 2, when removing the GAN losses and experimenting with only the four existing self-supervised losses, the evaluation results show a significant performance degradation in scene flow estimation. This demonstrates that introducing adversarial learning into scene flow estimation effectively improves scene flow estimation performance. Unlike other methods with self-supervised loss, SFGAN designs loss to self-supervise learn 3D scene flow by utilizing the difference between the distribution of generated data and real data. Finally, the average endpoint error (EPE3D) of scene flow is reduced to 0.098 without accessing scene flow annotations. The performance of scene flow estimation is also degraded by removing the Laplacian regularization loss and smoothing loss at the training process, respectively. The SFGAN framework still needs to be teamed with some existing losses to make the results optimal. As shown in Table 3, we try different loss weights W_{gan} . The training effect is better when W_{gan} takes the value of 2 or 3.



Figure 7: Interactive visualization of scene flow estimation. The point cloud of the first frame is shown in blue. The second frame of the point cloud is shown in green. The predicted point cloud of the second frame by our method is shown in red, and the predicted point cloud of the second frame by FlowNet3D is shown in purple.

In order to make the point cloud discriminator in adversarial learning correctly discriminate whether the input point cloud comes from the generated data or the real data, we propose four kinds of discriminators, as shown in Figure 4. As shown in Table 4, we perform ablation experiments for different point cloud discriminators. The best performance in scene flow estimation is achieved when PC_1 and PC_2^* perform flow embedding and the weights of the set conv layer are shared. This setup is more beneficial to improve the performance of scene flow estimation.



Figure 8: Interactive visualization of 3D point clouds. The real point cloud of the first frame is shown in blue. The real second frame of the point cloud is shown in green. The predicted point cloud of the second frame by our method is shown in red, and the predicted point cloud of the second frame by FlowNet3D is shown in purple.

Table 3: The effect of weight value W_{GAN} of GAN loss on scene flow estimation. The scene flow generator and the point cloud discriminator share the GAN loss weight values W_{GAN} in the respective back propagation. Models are self-supervised trained in FlyingThings3D and KITTI.

W_{GAN}	EPE3D↓	Acc3D Strict↑	Acc3D Relax↑	Outliers↓
1.0	0.1077	0.2520	0.6403	0.6555
2.0	0.0987	0.3022	0.6823	0.5584
3.0	0.1021	0.3205	0.6854	0.5532
4.0	0.1078	0.3167	0.6799	0.5604

Table 4: Ablation experiments of designing point cloud discriminators. The arrow direction means the direction of flow embedding. For example, ‘ $PC_1 \Rightarrow PC_2^*$ ’ means finding the softly corresponding points in PC_2^* for each point in PC_1 and learning the flow embedding for each point in PC_1 . ‘Shared’ indicates whether the set conv layer shares the weights, where the set conv layer is the feature extraction layer of the point cloud.

Embedding method	Shared	EPE3D↓	Acc3D Strict↑	Acc3D Relax↑	Outliers↑
$PC_2 \Rightarrow PC_2^*$ $PC_2^* \Rightarrow PC_2$	-	0.1155	0.1996	0.5928	0.6845
$PC_2 \Rightarrow PC_2^*$ $PC_2^* \Rightarrow PC_2$	✓	0.1048	0.2608	0.6673	0.5941
$PC_1 \Rightarrow PC_2^*$ $PC_1 \Rightarrow PC_2$	-	0.1021	0.2934	0.6768	0.5688
$PC_1 \Rightarrow PC_2^*$ $PC_1 \Rightarrow PC_2$	✓	0.0987	0.3022	0.6823	0.5584

Conclusion

In the paper, we propose a novel framework for self-supervised learning of scene flow, introducing adversarial learning methods in scene flow learning. We use the scene flow estimator as the scene flow generator G_{sf} , and design a new point cloud discriminator D_{pc} and corresponding GAN loss function. Experimental results demonstrate the effectiveness of adversarial learning for the task of scene flow estimation. No ground truth of scene flow is used in the training process of the scene flow estimation. The proposed method outperforms the baseline and some existing unsupervised learning methods in scene flow estimation on the real-world autonomous driving dataset, KITTI.

Acknowledgements

This work was supported in part by the Natural Science Foundation of China under Grant U1613218, Grant U1913204, and Grant 62073222; in part by the Shanghai Municipal Education Commission and Shanghai Education Development Foundation through the Shu Guang Project under Grant 19SG08; and in part by grants from the NVIDIA Corporation.

Conflict of interest

The authors report no conflicts of interest.

References

- Y. Almalioglu, Mru Saputra, Ppbd Gusmao, A. Markham, and N. Trigoni. GANVO: Unsupervised Deep Monocular Visual Odometry and Depth Estimation with Generative Adversarial Networks. In *2019 International Conference on Robotics and Automation (ICRA)*, 2019. doi: 10.1109/icra.2019.8793512.
- Aseem Behl, Omid Hosseini Jafari, Siva Karthik Mustikovela, Hassan Abu Alhaija, Carsten Rother, and Andreas Geiger. Bounding boxes, segmentations and object coordinates: How important is recognition for 3d scene flow estimation in autonomous driving scenarios? In *Proceedings of the IEEE International Conference on Computer Vision*, pages 2574–2583, 2017. doi: 10.1109/iccv.2017.281.
- J. Cech, J. Sanchez-Riera, and R. Horaud. Scene Flow Estimation by Growing Correspondence Seeds. In *IEEE Conference on Computer Vision & Pattern Recognition*, 2011. doi: 10.1109/cvpr.2011.5995442.
- A. X. Chang, T. Funkhouser, L. Guibas, P. Hanrahan, Q. Huang, Z. Li, S. Savarese, M. Savva, S. Song, and H. Su. ShapeNet: An Information-Rich 3D Model Repository. *Computer Science*, 2015.
- Andreas Geiger, Philip Lenz, and Raquel Urtasun. Are we ready for autonomous driving? The KITTI vision benchmark suite. In *2012 IEEE Conference on Computer Vision and Pattern Recognition*, pages 3354–3361, 2012. doi: 10.1109/CVPR.2012.6248074.
- I. J. Goodfellow, J. Pouget-Abadie, M. Mirza, B. Xu, D Warde-Farley, S. Ozair, A. Courville, and Y. Bengio. Generative Adversarial Networks. *Advances in Neural Information Processing Systems*, 3:2672–2680, 2014. doi: 10.1007/978-981-33-6048-8_1.
- X. Gu, Y. Wang, C. Wu, J. L. Yong, and P. Wang. HPLFlowNet: Hierarchical Permutohedral Lattice FlowNet for Scene Flow Estimation on Large-Scale Point Clouds. In *2019 IEEE/CVF Conference on Computer Vision and Pattern Recognition (CVPR)*, 2019. doi: 10.1109/cvpr.2019.00337.

- E. Herbst, X. Ren, and D. Fox. RGB-D flow: Dense 3-D motion estimation using color and depth. In *IEEE International Conference on Robotics & Automation*, 2013. doi: 10.1109/icra.2013.6630885.
- Frederic Huguet and Frederic Devernay. A Variational Method for Scene Flow Estimation from Stereo Sequences. In *2007 IEEE 11th International Conference on Computer Vision*, pages 1–7, 2007. doi: 10.1109/ICCV.2007.4409000.
- M. Jaimez, M. Souiai, J. Gonzalez-Jimenez, and D Cremers. A primal-dual framework for real-time dense RGB-D scene flow. In *IEEE International Conference on Robotics and Automation (ICRA)*, 2015. doi: 10.1109/icra.2015.7138986.
- Eunah Jung, Nan Yang, and Daniel Cremers. Multi-frame GAN: image enhancement for stereo visual odometry in low light. In *Conference on Robot Learning*, pages 651–660. PMLR, 2020.
- D. Kingma and J. Ba. Adam: A Method for Stochastic Optimization. *Computer Science*, 2014.
- Yair Kittenplon, Yonina C Eldar, and Dan Raviv. FlowStep3D: Model Unrolling for Self-Supervised Scene Flow Estimation. In *Proceedings of the IEEE/CVF Conference on Computer Vision and Pattern Recognition*, pages 4114–4123, 2021.
- Philip Lenz, Julius Ziegler, Andreas Geiger, and Martin Roser. Sparse scene flow segmentation for moving object detection in urban environments. In *2011 IEEE Intelligent Vehicles Symposium (IV)*, pages 926–932, 2011. doi: 10.1109/IVS.2011.5940558.
- Bing Li, Cheng Zheng, Silvio Giancola, and Bernard Ghanem. SCTN: Sparse Convolution-Transformer Network for Scene Flow Estimation. *arXiv preprint arXiv:2105.04447*, 2021a.
- Ruibao Li, Guosheng Lin, Tong He, Fayao Liu, and Chunhua Shen. HCRF-Flow: Scene Flow From Point Clouds With Continuous High-Order CRFs and Position-Aware Flow Embedding. In *Proceedings of the IEEE/CVF Conference on Computer Vision and Pattern Recognition (CVPR)*, pages 364–373, June 2021b.
- K. Liu, Q. Li, and G. Qiu. PoseGAN: A Pose-to-Image Translation Framework for Camera Localization. *ISPRS Journal of Photogrammetry and Remote Sensing*, 166:308–315, 2020. doi: 10.1016/j.isprsjprs.2020.06.010.
- X. Liu, C. R. Qi, and L. J. Guibas. FlowNet3D: Learning Scene Flow in 3D Point Clouds. In *2019 IEEE/CVF Conference on Computer Vision and Pattern Recognition (CVPR)*, 2019a. doi: 10.1109/cvpr.2019.00062.
- Xingyu Liu, Mengyuan Yan, and Jeannette Bohg. Meteornet: Deep learning on dynamic 3d point cloud sequences. In *Proceedings of the IEEE/CVF International Conference on Computer Vision*, pages 9246–9255, 2019b. doi: 10.1109/iccv.2019.00934.
- Nikolaus Mayer, Eddy Ilg, Philip Hausser, Philipp Fischer, Daniel Cremers, Alexey Dosovitskiy, and Thomas Brox. A Large Dataset to Train Convolutional Networks for Disparity, Optical Flow, and Scene Flow Estimation. In *Proceedings of the IEEE Conference on Computer Vision and Pattern Recognition (CVPR)*, June 2016. doi: 10.1109/cvpr.2016.438.
- M. Menze and A. Geiger. Object scene flow for autonomous vehicles. In *Computer Vision & Pattern Recognition*, 2015. doi: 10.1109/cvpr.2015.7298925.
- H. Mittal, B. Okorn, and D. Held. Just Go With the Flow: Self-Supervised Scene Flow Estimation. In *2020 IEEE/CVF Conference on Computer Vision and Pattern Recognition (CVPR)*, 2020. doi: 10.1109/cvpr42600.2020.01119.
- J. P. Pons, R. Keriven, and O. Faugeras. Multi-View Stereo Reconstruction and Scene Flow Estimation with a Global Image-Based Matching Score. *International Journal of Computer Vision*, 72(2):179–193, 2007. doi: 10.1007/s11263-006-8671-5.

- Jhony Kaesemodel Pontes, James Hays, and Simon Lucey. Scene Flow from Point Clouds with or without Learning. In *2020 International Conference on 3D Vision (3DV)*, pages 261–270, 2020. doi: 10.1109/3DV50981.2020.00036.
- Gilles Puy, Alexandre Boulch, and Renaud Marlet. Flot: Scene flow on point clouds guided by optimal transport. In *Computer Vision–ECCV 2020: 16th European Conference, Glasgow, UK, August 23–28, 2020, Proceedings, Part XXVIII 16*, pages 527–544. Springer, 2020. doi: 10.1007/978-3-030-58604-1_32.
- Charles R Qi, Hao Su, Kaichun Mo, and Leonidas J Guibas. Pointnet: Deep learning on point sets for 3d classification and segmentation. In *Proceedings of the IEEE conference on computer vision and pattern recognition*, pages 652–660, 2017a. doi: 10.1109/cvpr.2017.16.
- Charles Ruizhongtai Qi, Li Yi, Hao Su, and Leonidas J. Guibas. PointNet++: Deep Hierarchical Feature Learning on Point Sets in a Metric Space. *CoRR*, abs/1706.02413, 2017b. URL <http://arxiv.org/abs/1706.02413>.
- Deqing Sun, Xiaodong Yang, Ming-Yu Liu, and Jan Kautz. PWC-Net: CNNs for Optical Flow Using Pyramid, Warping, and Cost Volume. In *Proceedings of the IEEE Conference on Computer Vision and Pattern Recognition (CVPR)*, June 2018. doi: 10.1109/cvpr.2018.00931.
- Zachary Teed and Jia Deng. RAFT: Recurrent All-Pairs Field Transforms for Optical Flow. In Andrea Vedaldi, Horst Bischof, Thomas Brox, and Jan-Michael Frahm, editors, *Computer Vision – ECCV 2020*, pages 402–419, Cham, 2020. Springer International Publishing. ISBN 978-3-030-58536-5. doi: 10.24963/ijcai.2021/662.
- Zachary Teed and Jia Deng. RAFT-3D: Scene Flow Using Rigid-Motion Embeddings. In *Proceedings of the IEEE/CVF Conference on Computer Vision and Pattern Recognition (CVPR)*, pages 8375–8384, June 2021.
- Hugues Thomas, Charles R Qi, Jean-Emmanuel Deschaud, Beatriz Marcotegui, François Goulette, and Leonidas J Guibas. Kpconv: Flexible and deformable convolution for point clouds. In *Proceedings of the IEEE/CVF International Conference on Computer Vision*, pages 6411–6420, 2019. doi: 10.1109/iccv.2019.00651.
- Ivan Tishchenko, Sandro Lombardi, Martin R. Oswald, and Marc Pollefeys. Self-Supervised Learning of Non-Rigid Residual Flow and Ego-Motion. In *2020 International Conference on 3D Vision (3DV)*, pages 150–159, 2020. doi: 10.1109/3DV50981.2020.00025.
- Guangming Wang, Yehui Yang, Huixin Zhang, Zhe Liu, and Hesheng Wang. Spherical Interpolated Convolutional Network with Distance-Feature Density for 3D Semantic Segmentation of Point Clouds. *arXiv preprint arXiv:2011.13784*, 2020a.
- Guangming Wang, Chi Zhang, Hesheng Wang, Jingchuan Wang, Yong Wang, and Xinlei Wang. Unsupervised learning of depth, optical flow and pose with occlusion from 3d geometry. *IEEE Transactions on Intelligent Transportation Systems*, 2020b. doi: 10.1109/tits.2020.3010418.
- Guangming Wang, Yunzhe Hu, Xinrui Wu, and Hesheng Wang. Residual 3D Scene Flow Learning with Context-Aware Feature Extraction. *arXiv preprint arXiv:2109.04685*, 2021a.
- Guangming Wang, Hanwen Liu, Muyao Chen, Yehui Yang, Zhe Liu, and Hesheng Wang. Anchor-Based Spatio-Temporal Attention 3D Convolutional Networks for Dynamic 3D Point Cloud Sequences. *IEEE Transactions on Instrumentation and Measurement*, pages 1–1, 2021b. doi: 10.1109/TIM.2021.3106101.
- Guangming Wang, Shuaiqi Ren, and Hesheng Wang. NccFlow: Unsupervised Learning of Optical Flow With Non-occlusion from Geometry. *arXiv preprint arXiv:2107.03610*, 2021c.
- Guangming Wang, Xinrui Wu, Zhe Liu, and Hesheng Wang. Hierarchical Attention Learning of Scene Flow

in 3D Point Clouds. *IEEE Transactions on Image Processing*, 30:5168–5181, 2021d. doi: 10.1109/TIP.2021.3079796.

Guangming Wang, Xinrui Wu, Zhe Liu, and Hesheng Wang. PWLO-Net: Deep LiDAR Odometry in 3D Point Clouds Using Hierarchical Embedding Mask Optimization. In *Proceedings of the IEEE/CVF Conference on Computer Vision and Pattern Recognition*, pages 15910–15919, 2021e.

Pichao Wang, Wanqing Li, Zhimin Gao, Yuyao Zhang, Chang Tang, and Philip Ogunbona. Scene flow to action map: A new representation for rgb-d based action recognition with convolutional neural networks. In *Proceedings of the IEEE Conference on Computer Vision and Pattern Recognition*, pages 595–604, 2017. doi: 10.1109/cvpr.2017.52.

W. Wu, Z. Y. Wang, Z. Li, W. Liu, and F. Li. *PointPWC-Net: Cost Volume on Point Clouds for (Self-)Supervised Scene Flow Estimation*. *Computer Vision – ECCV 2020*, 2020. doi: 10.1007/978-3-030-58558-7_6.

Wenxuan Wu, Zhongang Qi, and Li Fuxin. PointConv: Deep Convolutional Networks on 3D Point Clouds. In *2019 IEEE/CVF Conference on Computer Vision and Pattern Recognition (CVPR)*, pages 9613–9622, 2019. doi: 10.1109/CVPR.2019.00985.

Guangyao Zhai, Xin Kong, Jinhao Cui, Yong Liu, and Zhen Yang. FlowMOT: 3D Multi-Object Tracking by Scene Flow Association. *arXiv preprint arXiv:2012.07541*, 2020.